Journal of Mining and Environment (JME), Vol. 12, No. 2, 2021, 547-567

Shahrood University of Technology

Iranian Society of Mining Engineering (IRSME)

Journal of Mining and Environment (JME)

journal homepage: www.jme.shahroodut.ac.ir

THOMSON REUTERS

Stable Downward Continuation of Airborne Potential Field Geophysical Data: an Investigation of Stabilizer Family

Majid Azadi, Maysam Abedi* and Gholam-Hossain Norouzi

School of Mining Engineering, College of Engineering, University of Tehran, Tehran, Iran

Article Info

Received 19 April 2021

Received in Revised form 14 May 2021

Accepted 21 May 2021

Published online 21 May 2021

DOI:10.22044/jme.2021.10740.2040

Keywords

Signal attenuation

Stable downward continuation

Tikhonov regularization

Stabilizing functions

Abstract

Attenuation of the signal received from the sources causing anomalies is the negative feature of the airborne measurements. Using a stable downward continuation method is a practical way to address this shortcoming. In this work, we investigate the efficiency of various stabilizers in achieving a stable downward continued data. The purpose of this work is to select the most appropriate stabilizer(s) for this operation. We examine the various stabilizing functions by introducing them into the Tikhonov regularization problem. The results of the research work on the synthetic airborne gravity and magnetic data show that the βL1 (the other definition of L1 norm) and SM (the smoothest model) stabilizers have the potential to be used in the stable implementation of the downward continuation method. These stabilizers perform better than the others in the three comparisons including the visual, quantitative (RMS error), and graphical comparisons. Also by examining the airborne magnetic data related to the Esfordi district in the Yazd Province (Iran), it has been found that, in general, the βL1 stabilizer is more suitable than the other stabilizing functions studied in this research work.

1. Introduction

Nowadays, the importance of using airborne surveys, especially in mineral exploration, is not hidden from anyone. In the early stages of exploration, i.e. the reconnaissance stage, aerial surveys help us to limit large areas, and achieve promising smaller areas (prospects). In addition, the rapid implementation and cost-effective coverage of large areas and the facilitation of data measurement in impassable areas are some of our incentives to use the airborne surveying method [1, 2]. Unfortunately, despite these advantages, the received signals are weakened due to the distance from the sources causing the anomalies. Also the data resolution reduces such that distinguishing different sources from each other is not easily possible. In these cases, a downward continuation method has been used in order to address these shortcomings and achieve a better interpretable data.

The downward continuation method is the mathematical projection of the potential field data (gravity or magnetic) from one datum vertically downwards to another datum [3]. This method increases the perceptibility of the small, shallow-sourced anomalies over that of the original data [4]. Nevertheless, this operation is unstable, and the presence of noise in the original data is troublesome; therefore, like the inverse modeling method, it is considered as an ill-posed problem. In order to stabilize the calculations related to this operation, different methods have been proposed, in which the stable downward continued data is usually produced by the directed or iteration method [5]. Among them, the Tikhonov regularization-based method and its high applicability have been investigated in many studies (e.g. [6-9]). (Note that the Tikhonov regularization method was first described by Tikhonov and Arsenin (1977) [10], and the readers

* *Corresponding author: maysamabedi@ut.ac.ir (M. Abedi).*

can refer to it for a further understanding.) In fact, in this approach, the stable downward continuation operation is simulated by inverting the original data in the Fourier domain. Then in order to solve the new problem, the corresponding Tikhonov cost function is minimized. This function consists of data misfit and model norms. The data misfit norm, which controls the extent to which the data fits the model, has a single definition in most studies, i.e. the sum of the squares of the difference between the recovered and measured data. However, the model norm term is chosen in order to meet the available information and assumptions related to the desired solution. The previous inversion algorithms used the L_2 norm as the model norm. Although this choice had the advantage of simplifying the calculations, it produced smooth solutions that were, in some cases, far from the truth. Then in order to eliminate the existing gaps and achieve models closer to reality, various stabilizing functions have been introduced by many researchers. For example, in [11-15], the minimum support (MS), smoothest model (SM), total variation (TV), first-order minimum entropy (ME-1), and minimum gradient support (MGS) stabilizers have been introduced, respectively. The stabilizing function plays an essential role in solving the inverse problem by selecting the most appropriate model from the set of possible ones [16]. For instance, the L_2 norm and maximum smoothness stabilizers produce smooth solutions, while the minimum gradient support, minimum support, total variation, and minimum entropy are used to create non-smooth solutions. Also, blocky and piecewise-constant results can be produced using the L_1 norm. The use of stabilizers in the inversion of various geophysical data is common (e.g. [17, 18] (2D magnetotelluric data); [19] (gravity and magnetic data); [20] (1D and 2D magnetotelluric data); [21] (3D DC resistivity data), and [22] (3D gravity data)).

This work aims to investigate the performance of some stabilizers in the production of stable downward continued data. We will answer the following questions: Will different stabilizers be able to do this operation at all? Will the use of different stabilizers in this problem produce different results? We will use the stabilizers including the L_1 norm, L_2 norm, SM, MS, MGS, ME-1, and TV. In the following, implementing the proposed method is explained by describing the stabilization of downward continuation using the Tikhonov method, and then introducing the mentioned stabilizing functions and how to incorporate them into the inversion problem.

2. Methodology

Our proposed method for stabilizing the calculations of downward continuation is based on the Tikhonov regularization method, and is performed using the mentioned stabilizers. The definitions and mathematics of our method are concisely explained in the following sub-sections.

2.1. Stable downward continuation

In physical terms, the downward continued filter transforms the data to what it would have been if the measurements had been made at a different height below the observational level [23]. The data obtained at two different elevation levels are related to each other by Equation (1), as follows [24-27]:

$$P_{z_2}(x,y,\Delta z)=\frac{1}{2\pi}\iint_{-\infty}^{+\infty}\frac{P_{z_1}(X,Y)\Delta z}{[(X-x)^2+(Y-y)^2+\Delta z^2]^{3/2}}dXdY\ ,\Delta z=z_2-z_1\geq 0 \quad (1)$$

This equation represents the upward continuation operation in an integral form of convolution, where P_{z_1} and P_{z_2} are, respectively, the potential field data at two distinct elevation levels located at vertical distance Δz from each other, (X,Y,z_1) and (x,y,z_2) represent the coordinates of the data at the lower and upper height levels, respectively. Transferring the data from the spatial domain to the spectral domain using 2D Fourier transform produces the following more straightforward relation:

$$\tilde{P}_{z_2}(K_x,K_y,\Delta z)=e^{-\Delta zK}\tilde{P}_{z_1}(K_x,K_y) \quad (2)$$

where $\tilde{P}$ represents the Fourier transform of P, $e^{-\Delta zK}$ is the upward continuation operator, $K=\sqrt{K_x^2+K_y^2}$ is the radial wavenumber, and K_x and K_y are the wave numbers in the x and y directions, respectively. Since the measured data is often noisy, the stable execution of the downward continuation operation is challenging. The Tikhonov regularization method has often been a practical solution to this problem (e.g. [5, 6, and 28]). Here, we describe the following inversion problem, relying on Abedi *et al.* (2013), who have simulated the stable downward continuation

operation by the airborne data inversion in the Fourier domain [6].

From the similarity of Equation (2) with the forward modeling problem, it is inferred that the stable downward continued data can be calculated by inverting the airborne data (in the Fourier domain):

$$\left[\tilde{d}_{up}\right]_{n\times 1} = G_{n\times n}\left[\tilde{d}_{down}\right]_{n\times 1} \quad (3)$$

where $\tilde{d}_{up}$ and $\tilde{d}_{down}$ are the airborne potential data and the corresponding downward continued data in Fourier domain, respectively. The forward operator G is a diagonal matrix containing the values of $e^{-\Delta zK}$. In order to solve the inverse problem, the following Tikhonov parametric function (P^{α}) is minimized:

$$P^{\alpha}(m,d) = \phi(m,d) + \lambda S(m) \quad (4)$$

where $\phi(m,d)$ and $S(m)$ represent the data misfit and the stabilizing functions, respectively, m shows the desired solution, and d is the measured data that here is equivalent to $\tilde{d}_{down}$ and $\tilde{d}_{up}$, respectively. The data misfit function is defined as follows:

$$\phi(m,d) = \left\|\left(\boldsymbol{d} - \boldsymbol{G}(m)\right)\right\|_2^2 \quad (5)$$

The regularization parameter λ plays a controlling role in the importance of these terms on the inversion results. Several methods have been proposed for automatically estimating this parameter, and the L-curve method is used in this work. In this method, the curve is obtained by plotting the solution norm against the corresponding residual norm for different regularization parameters in the logarithmic scale. Then the elbow point represents the optimal regularization parameter [29]. The following sub-section provides more details about the stabilizing term.

2.2. Stabilizers family

The main application of the stabilizing functions is to select solutions from a set of possible ones that are continuously dependent on the data, and have particular properties according to the selected function [16]. In the following, the stabilizers used in this work are introduced, and their equations are presented:

The L_1 norm stabilizer is defined in the following form:

$$S_{L_1}(m) = \sum_{i=1}^{M} |m_i| \quad (6)$$

where m_i represents the model parameter. This function can also be re-written as follows, the advantage of which will be determined later. In order to distinguish between these definitions, we display the second definition with $S_{\beta L_1}(m)$.

$$S_{\beta L_1}(m) = S_{L1}(m) = \sum_{i=1}^{M} \frac{|m_i|}{|m_i|}|m_i| = \sum_{i=1}^{M} \frac{{m_i}^2}{\sqrt{{m_i}^2}} \cong \sum_{i=1}^{M} \frac{{m_i}^2}{\sqrt{{m_i}^2 + \beta^2}} \quad (7)$$

where β is a very small positive value.

The L_2 norm stabilizer is defined as the square root of the sum of the squares of the model parameters, i.e.

$$S_{L_2}(m) = \left(\sum_{i=1}^{M} |m_i|^2\right)^{1/2} \quad (8)$$

The next stabilizing function is the smoothest model (SM), given below as:

$$S_{SM}(m) = \|\nabla^2 m\|^2 \quad (9)$$

where ∇ is the gradient operator here and in the subsequent cases. The two functions, minimum support (MS), and minimum gradient support (MGS) used in focusing inversion are written as follow:

$$S_{MS}(m) = \sum_{i=1}^{M} \frac{{m_i}^2}{{m_i}^2 + \beta^2} \quad (10)$$

$$S_{MGS}(m) = \sum_{i=1}^{M} \frac{\nabla m_i \nabla m_i}{\nabla m_i \nabla m_i + \beta^2} \quad (11)$$

where β is called a focusing parameter, and is selected as a small positive number.

The next stabilizer creating sharp models in inversion is called the first-order minimum entropy (ME-1), which is defined as follows:

$$S_{ME-1}(m) = -\sum_{i=1}^{M-1}\left[\frac{|m_{i+1} - m_i| + \beta}{\sum_{i=1}^{M-1}(|m_{i+1} - m_i| + \beta)} . log\left(\frac{|m_{i+1} - m_i| + \beta}{\sum_{i=1}^{M-1}(|m_{i+1} - m_i| + \beta)}\right)\right] \quad (12)$$

The last stabilizer whose impact on performing stable downward continuation of airborne data is investigated is the total variation function (TV).

$$S_{TV}(m) = \sum_{i=1}^{M} \frac{|\nabla m_i| + \beta^2}{\sqrt{(m_i + \beta^2)}} \quad (13)$$

In the last two cases, β is selected as an infinitesimal small positive constant.

Fortunately, all the stabilizing functions can be re-written as a pseudo-quadratic function of the model parameters. This procedure makes it easy to solve the optimization problem, and creates a single method in order to achieve the desired solution. Accordingly, the parametric function is re-written as Equation (14):

$$P^{\alpha}(m,d) = \left\|\left(\boldsymbol{d} - \boldsymbol{G}(m)\right)\right\|_2^2 + \lambda\|\boldsymbol{W}\boldsymbol{m}\|_2^2 \quad (14)$$

where $\boldsymbol{W}$ is the product of two variables ($\boldsymbol{w_e}$) and constant ($\boldsymbol{L}$) weighting matrices, i.e.

$$\boldsymbol{W} = \boldsymbol{w_e}\boldsymbol{L} \quad (15)$$

In this relation, $\boldsymbol{w_e}$ is the pseudo-quadratic form of the selected stabilizing function, and according to this choice, the matrix $\boldsymbol{L}$ is chosen as zero, the first or second derivative of the potential field in the z direction. The n vertical derivative of the potential field data in the Fourier domain is calculated through:

$$F\left[\frac{d^n P}{dz^n}\right] = |K|^n F[P] \quad (16)$$

where F represents the Fourier transform operator, P is the potential field data, and K is the radial wave number. Accordingly, the operator L can be obtained by evaluating $|K|^n$. Here, the $\boldsymbol{L}$ matrix corresponding to the βL$_1$, L$_2$, and ME-1 stabilizers equal to the identity matrix (i.e. $\boldsymbol{L} = \boldsymbol{I}$) for L$_1$, MS, MGS, and TV equal to K and in relation to the SM stabilizer equal to K^2.

The $\boldsymbol{w_e}$ equations for different stabilizers have been introduced in various studies (e.g. [16, 21]). Table 1 shows these relations. Since these weighting functions depend on the model parameters, the inverse problem is required to be solved by iteration.

Table 1. Pseudo-quadratic forms corresponding to various stabilizers; j is the iteration number, β is a very small positive value, ∇ is the gradient operator, and m_j represents the model parameter in *the* jth iteration [21].

Stabilizer	Notation	W_{e_j}	
1-norm (definition 1)	βL$_1$	$W_{e_j}^{\beta L_1} = diag\left(\frac{1}{\left(\boldsymbol{m}_j{}^2 + \beta^2\right)^{1/4}}\right)$	(17)
1-norm (definition 2)	L$_1$	$W_{e_j}^{L_1} = diag\left(\boldsymbol{m}_j\right)$	(18)
2-norm	L$_2$	$W_{e_j}^{L_2} = diag\left(\boldsymbol{m}_j{}^2\right)$	(19)
smoothest model	SM	$W_{e_j}^{SM} = diag\left(\nabla\boldsymbol{m_j}.\nabla\boldsymbol{m_j}\right)$	(20)
Minimum support	MS	$W_{e_j}^{MS} = diag\left(\frac{1}{\left(\boldsymbol{m}_j{}^2 + \beta^2\right)^{1/2}}\right)$	(21)
Minimum gradient support	MGS	$W_{e_j}^{MGS} = diag\left(\frac{\nabla\boldsymbol{m}_j}{\left(\left(\nabla\boldsymbol{m}_j\right)^2 + \beta^2\right)^{1/2}\left(\boldsymbol{m}_j{}^2 + \beta^2\right)^{1/2}}\right)$	(22)
Minimum entropy-1	ME-1	$W_{e_j}^{ME1} = diag\left[-\left(\frac{\lvert m_{i+1} - m_i\rvert + \beta}{\sum_{i=1}^{M-1}(\lvert m_{i+1} - m_i\rvert + \beta)}\right).log\left(\frac{\lvert m_{i+1} - m_i\rvert + \beta}{\sum_{j=1}^{M-1}(\lvert m_{i+1} - m_i\rvert + \beta)}\right)\frac{1}{(m_i{}^2 + \beta^2)^{1/2}}\right]$	(23)
Total variation	TV	$W_{e_j}^{TV} = diag\left(\frac{\lvert\nabla\boldsymbol{m}_j\rvert^2 + \beta^2}{\left(\boldsymbol{m}_j{}^2 + \beta^2\right)^{1/2}}\right)$	(24)

The desired solution is obtained as the following iterative procedure:

$$\tilde{d}_{down}^{j+1} = (G^T G + \lambda (w_e{}^T)^j w_e{}^j L^T L)^{-1} G^T \tilde{d}_{up} \quad (25)$$

$$j = 0, 1, 2, \ldots$$

where T represents the transpose of a matrix. For the first iteration ($j = 0$), we considered the w_e matrix equal to the identity matrix. In the later iterations, this matrix is assessed using the model parameters gained in the former iteration. The following relation is considered as the stop criterion for the iterations.

$$\|\tilde{d}_{down}^{j+1} - \tilde{d}_{down}^{j}\|_2^2 / \|\tilde{d}_{down}^{j}\|_2^2 \leq tolerance \quad (26)$$

3. Application to synthetic potential field data

In order to evaluate the capability of the mentioned stabilizers in the successful implementation of stable downward continuation, the synthetic models of gravity and magnetic were simulated with the physical characteristics summarized in Table 2. These models consist of seven rectangular prisms in which four blocks are large-sized targets, and three blocks represent the small-sized ones (Figures 1c and 1f). The Earth magnetic field was assumed by a vector with an inclination I = 50°, a declination D = 2°, and a strength of 46,000 nT. By the forward modeling method, 10201 data points were generated at an altitude of 150 m on a 100 m grid spacing over a survey area of 1 km by 1 km. This airborne gravity and magnetic data are shown in Figures 1a and 1d, respectively. The theoretical observations at the ground level were also created in order to evaluate the stable downward continuation operation (Figures 1b and 1e). Also, to get closer to the actual situation, the surface and airborne data was corrupted with 2% and 3% Gaussian noise, respectively, for the gravity and magnetic data.

Table 2. The assumed parameters for the synthetic models shown in Figures. 1c and 1f.

Model	Dimension (m)	Depth (m)	Susceptibility (SI)	Density contrast (g/cm^3)
1	1000 × 3000 × 500	500	0.06	0.5
2	500 × 500 × 150	50	0.06	0.5
3	500 × 1000 × 200	100	0.06	0.5
4	750 × 500 × 150	150	0.06	0.5
5	100 × 100 × 75	50	0.1	1.5
6	100 × 150 × 100	75	0.08	1
7	200 × 100 × 75	25	0.06	0.5

As it can be seen, due to the geophysical signal attenuation, none of the small-sized targets is evident within the airborne anomalies clearly, and their manifestations are very weak (Figures. 1a and 1d). In contrast, those targets have significant signatures in the surface data (Figures. 1b and 1e). The stable downward continuation of airborne data was performed using eight different stabilizers (βL$_1$, L$_1$, L$_2$, SM, MS, MGS, ME-1, and TV) with the method described in Section 2.1. The final parameters used in the desired approach are given in Table 3. As shown in this table, the ***L*** matrix used in the different methods is not the same. We examined different modes in order to find the most suitable matrix, and in fact, the expressed matrix produced the best results.

Table 3. The parameters used for downward continuation of the synthetic data.

Stabilizer	w_e matrix	β	*L* matrix	λ	
				Magnetic	Gravity
βL1	Eq. (17)	10^{-3}	I	4.84	2.50e(-1)
L1	Eq. (18)	-	K	2.25e(-6)	2.50e(-3)
L2	Eq. (19)	-	I	2.50e(-3)	1.60e(-3)
SM	Eq. (20)	-	K^2	4.90e(+7)	9.00e(+6)
MS	Eq. (21)	10^{-3}	K	8.10e(+5)	9.00e(+4)
MGS	Eq. (22)	10^{-10}	K	2.89e(-6)	2.50e(-3)
ME-1	Eq. (23)	10^{-15}	I	1.68e(-5)	1.44e(-4)
TV	Eq. (24)	10^{-15}	K	3.18e(-7)	4.20e(-3)

Based on this, the airborne gravity and magnetic data was transferred from a height of 150 m to the ground surface. Figures 2 and 5 show the results obtained for the magnetic and gravity data, respectively. These results were generated from the optimal regularization parameter selected from the

L-curve method (Figures 3 and 6). These values are also listed in Table 3.

In order to evaluate the performance of different stabilizers, 150 m-downward continued data was compared with the surface theoretical data using the same color legend bar to facilitate visual comparison. The visual comparisons of data in magnetic (i.e. Figure 2 *vs.* Figure 1d) and gravity case (i.e. Figure 5 *vs.* Figure 1e) indicate that different stabilizers have performed stable downward continued data satisfactorily. However, the results obtained from some stabilizers are flawed so that smaller sources have less resolution, and in some cases, additional noise is introduced into the data.

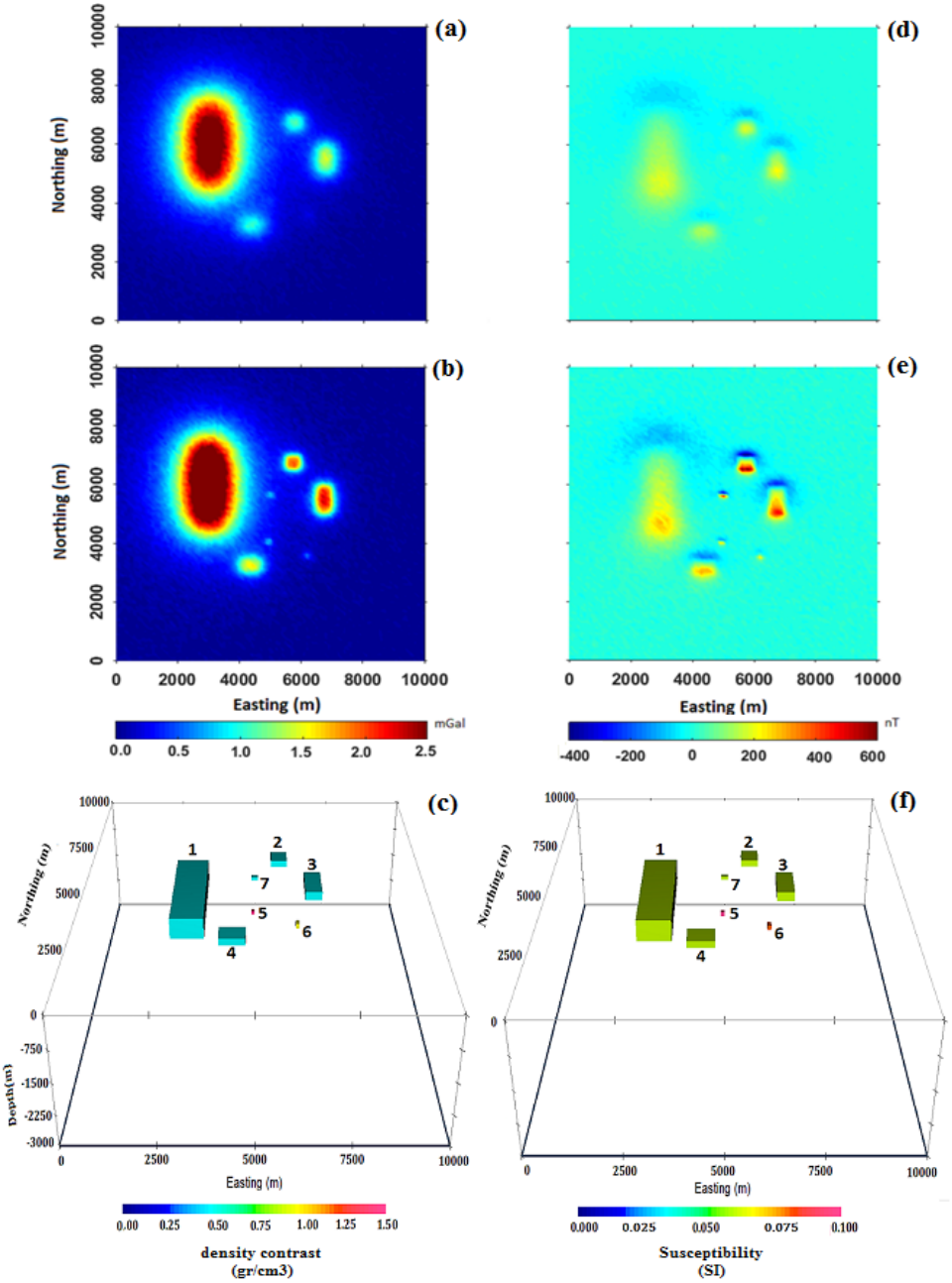

Figure 1. Synthetic potential field data simulation (a) gravity data at an altitude of 150 m, (b) gravity data at surface, (c) geometry of multi-source anomaly with different density contrasts, (d) magnetic data at an altitude of 150 m, (e) magnetic data at surface, and (f) geometry of multi-source anomaly with different magnetic susceptibility. Both surface and airborne data were corrupted with 2% and 3% Gaussian noise, respectively, for the gravity and magnetic data.

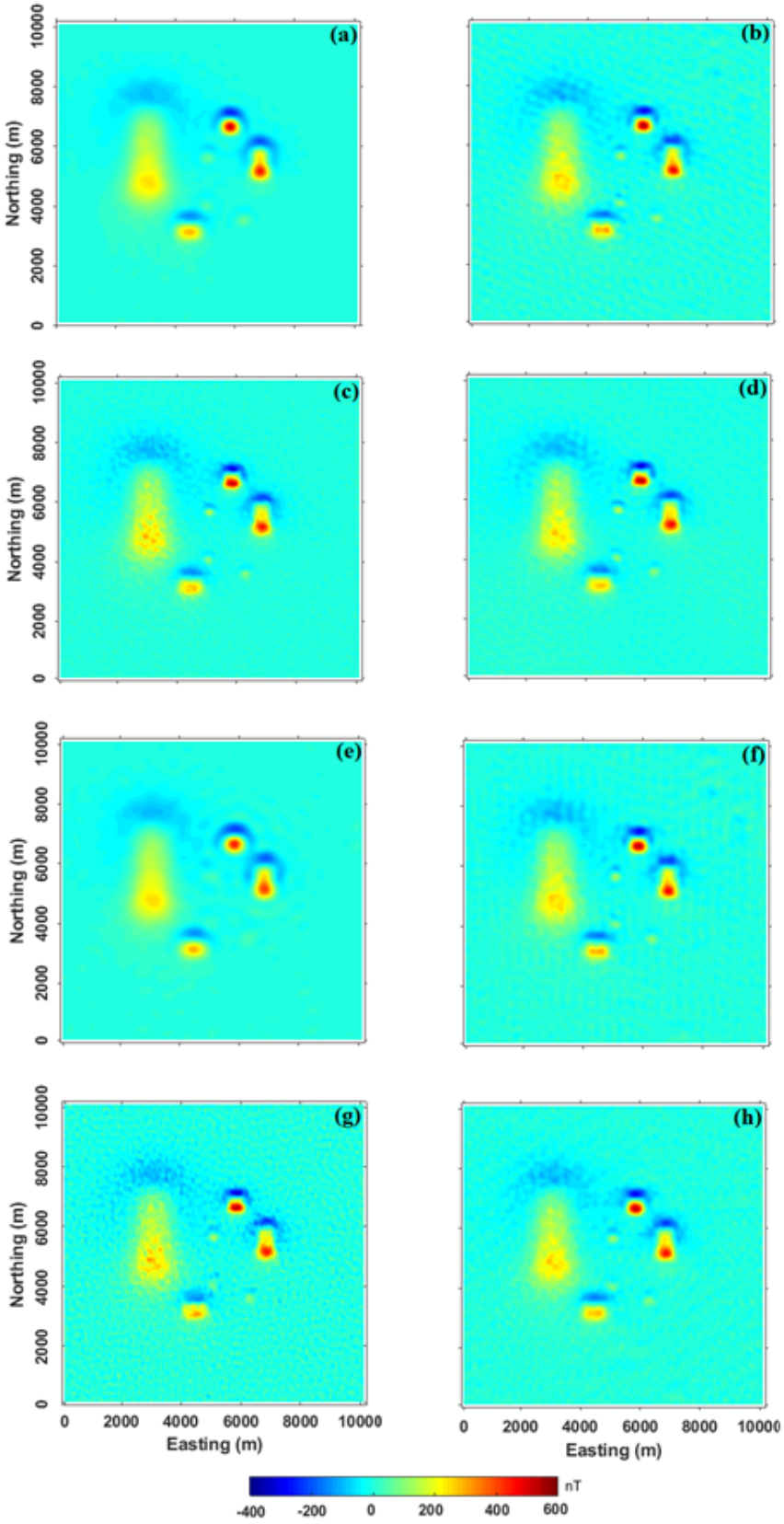

Figure 2. Downward continuation of the synthetic magnetometry data with various stabilizers from an altitude of 150 m to the ground surface through implementing a stabilizer of (a) βL1, (b) L1, (c) L2, (d) SM, (e) MS, (f) MGS, (g) ME-1, and (h) TV.

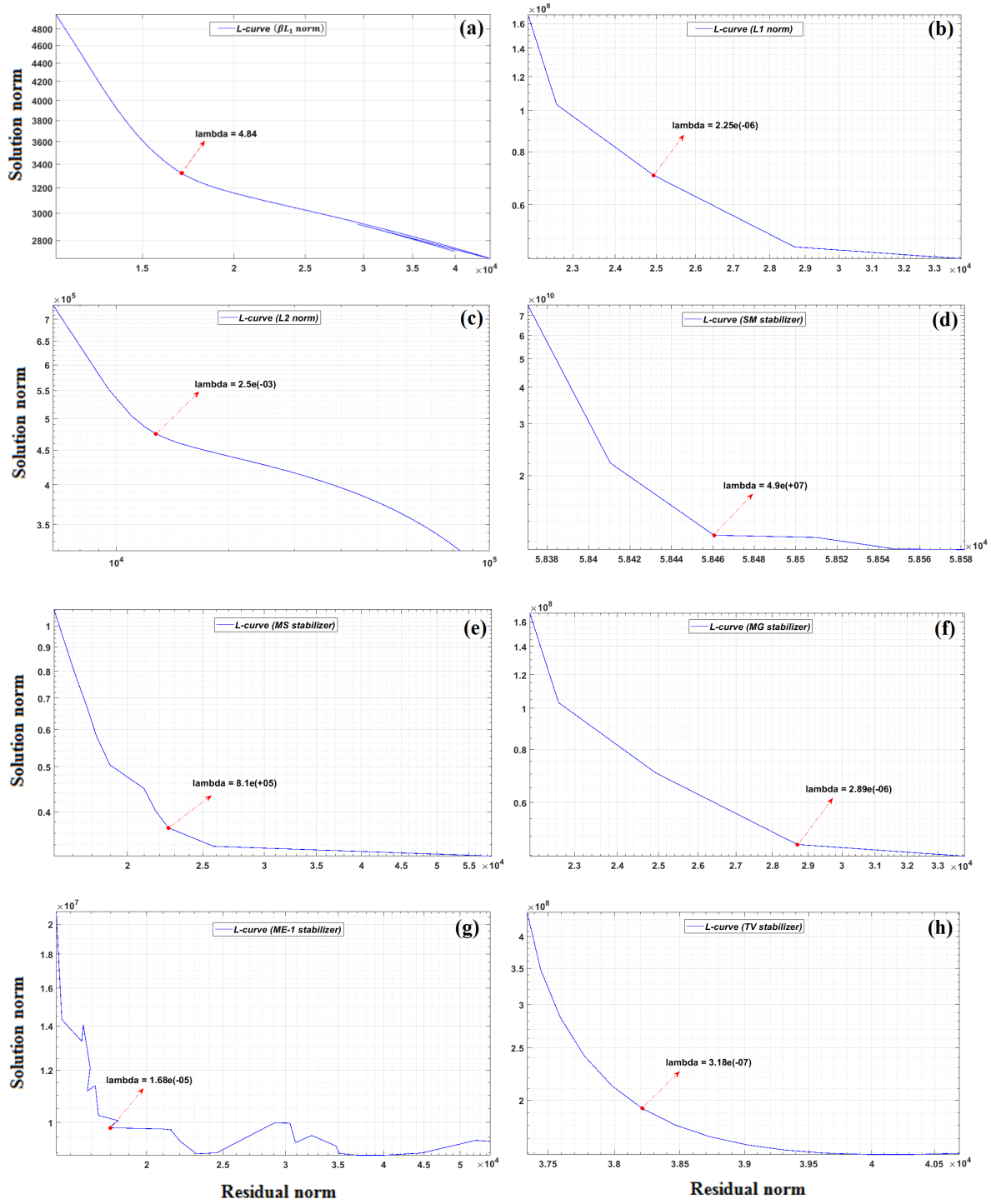

Figure 3. Selection of an optimum regularization parameter by means of L-curve method for the various stabilizers of (a) βL1, (b) L1, (c) L2, (d) SM, (e) MS, (f) MGS, (g) ME-1, and (h) TV. The corresponding downward continued magnetic data is presented in Figure 2.

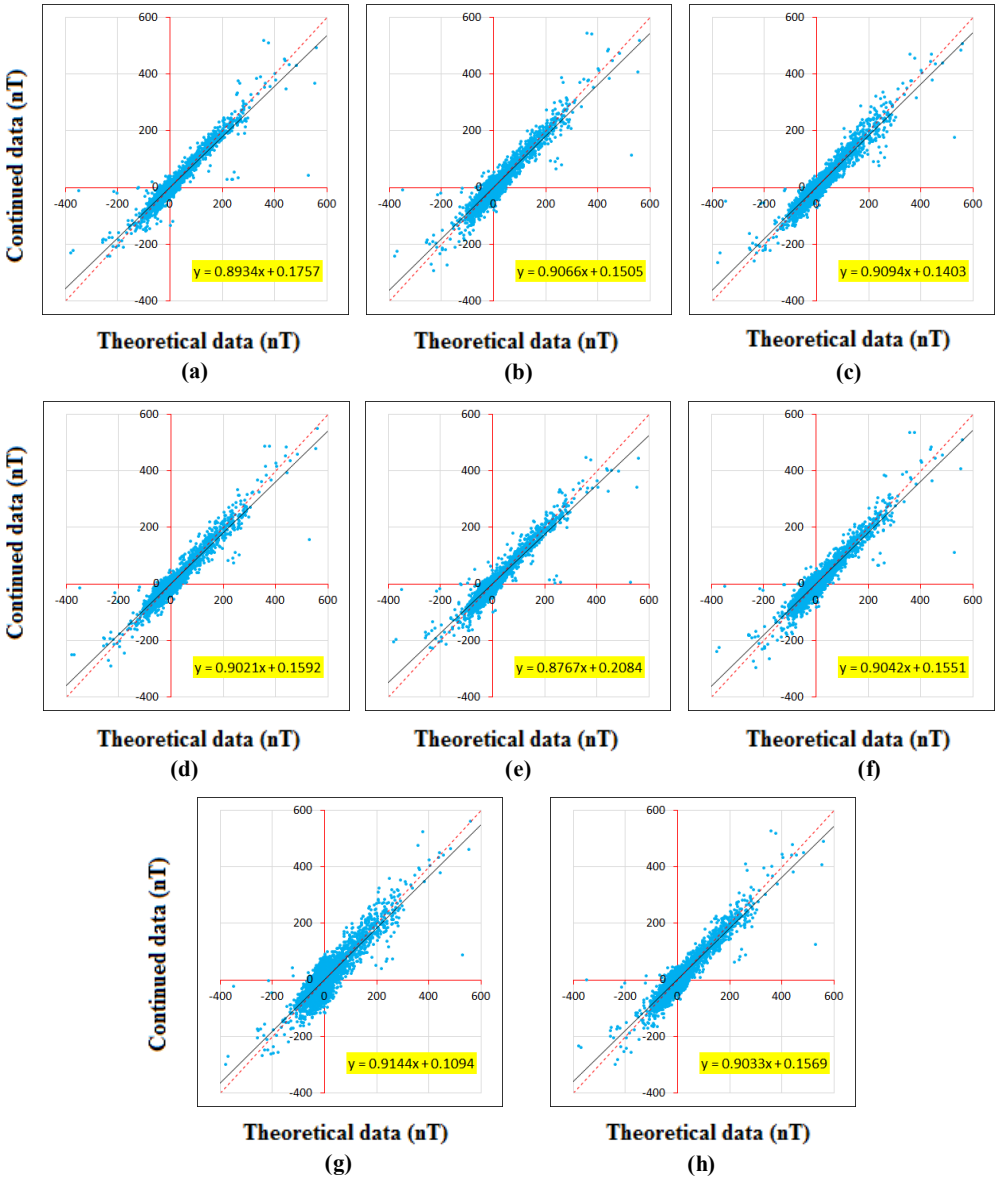

Figure 4. Plot of the 150-m downward continued synthetic magnetic data versus the theoretical data for the various stabilizers of (a) βL_1, (b) L_1, (c) L_2, (d) SM, (e) MS, (f) MGS, (g) ME-1, and (h) TV.

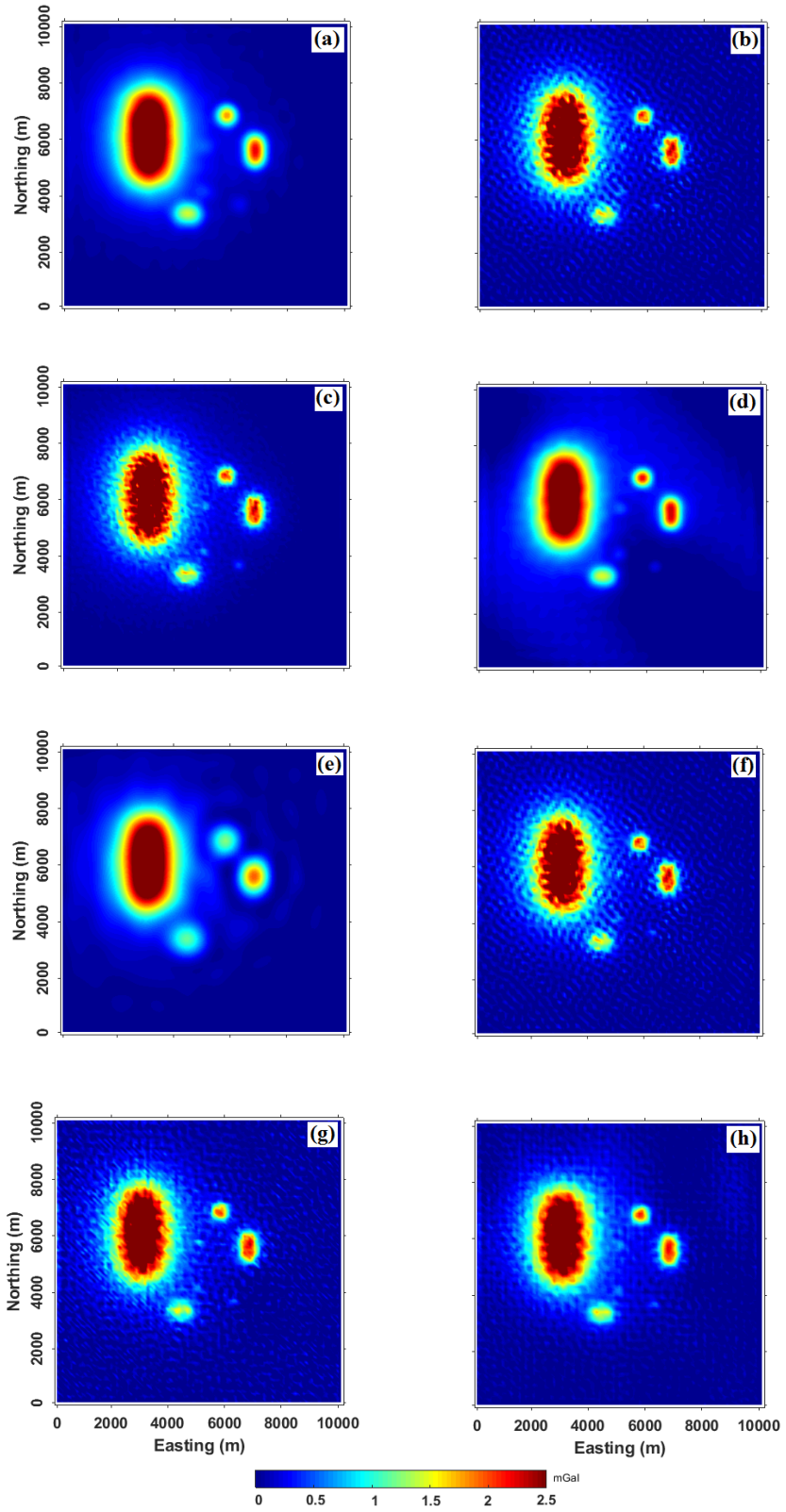

Figure 5. Downward continuation of the synthetic gravity data with various stabilizers from an altitude of 150 m to the ground surface through implementing a stabilizer of (a) βL_1, (b) L_1, (c) L_2, (d) SM, (e) MS, (f) MGS, (g) ME-1, and (h) TV.

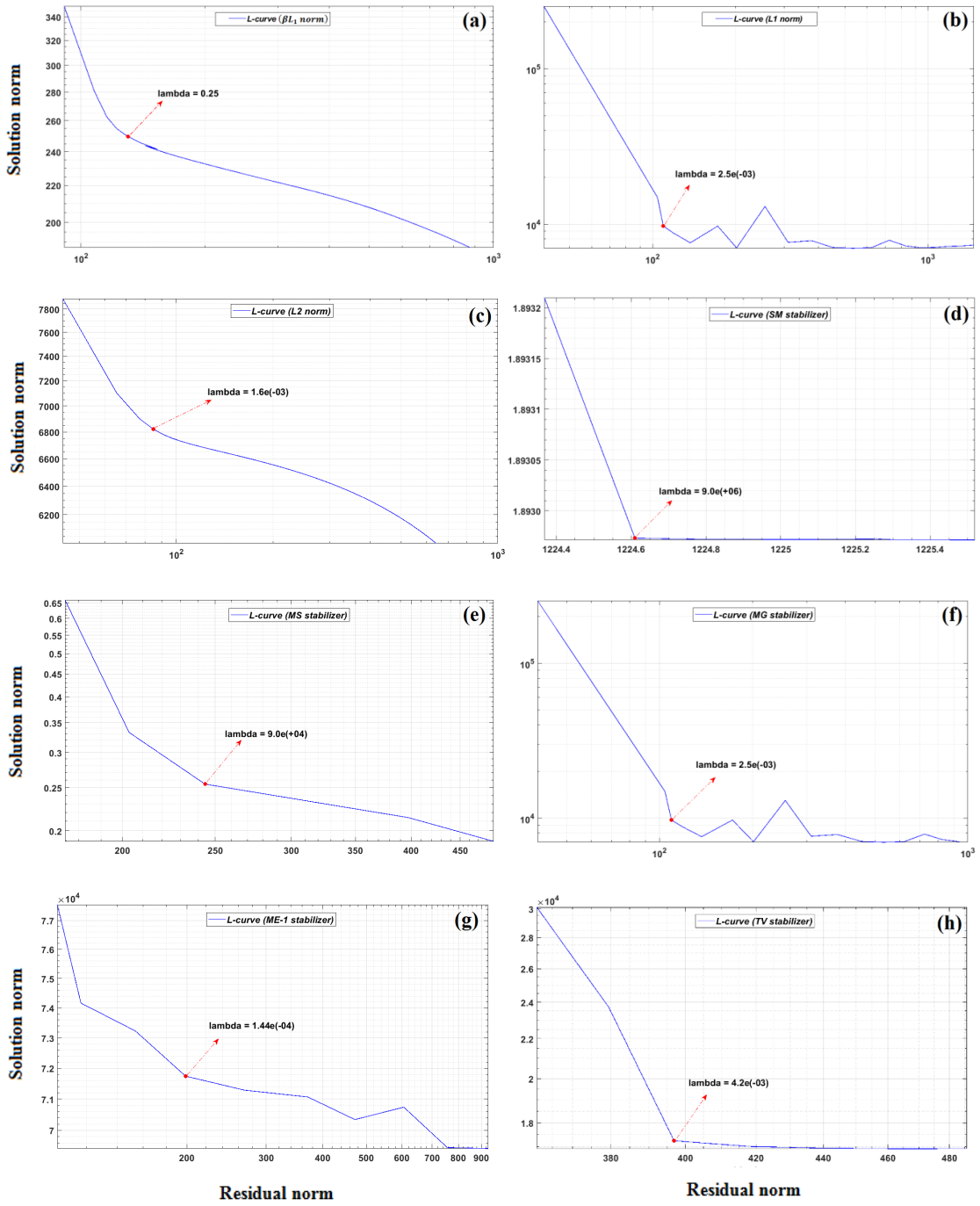

Figure 6. Selection of an optimum regularization parameter by means of L-curve method for the various stabilizers of (a) βL_1, (b) L_1, (c) L_2, (d) SM, (e) MS, (f) MGS, (g) ME-1, and (h) TV. The corresponding downward continued gravity data is presented in Figure 5.

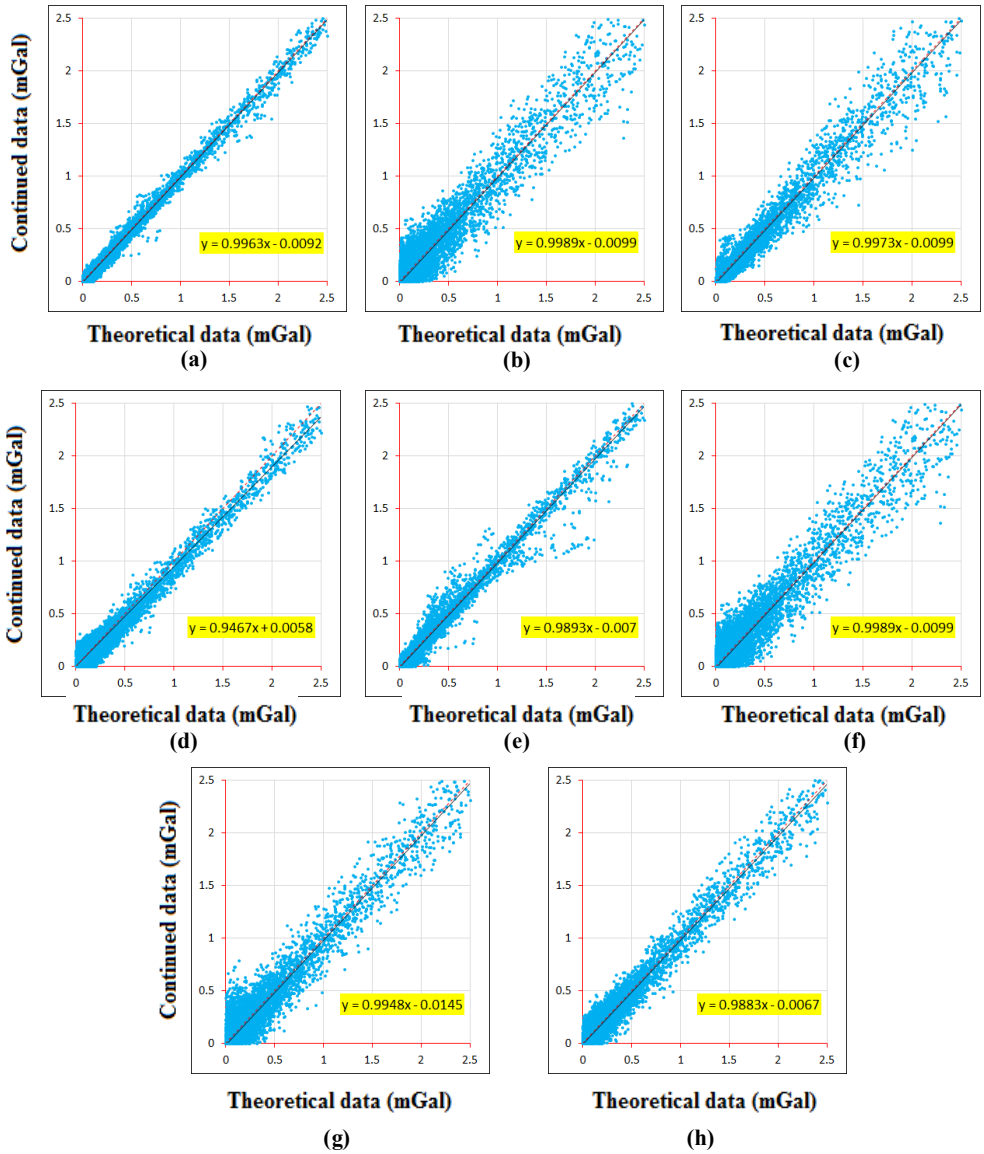

Figure 7. Plot of the 150-m downward continued synthetic gravity data versus the theoretical data for the various stabilizers of (a) βL_1, (b) L_1, (c) L_2, (d) SM, (e) MS, (f) MGS, (g) ME-1, and (h) TV.

For example, in the magnetic case, in Figure 2e (MS stabilizer), the anomalous areas related to small sources are less clear. Also in Figures. 2b and 2g, which are related to the L_1 and ME-1 stabilizers, respectively, the amount of noise is high, and causes a weakening in the display. Also in the gravity data, the evidence of the presence of all sources appears in all images (except Figure 5e). Figures. 5a, 5c, 5d, and 5h, which are the results for the βL_1, L_2, SM, and TV stabilizers, respectively, prove the existence of sources, while controlling the noise level. In addition, in order to quantitatively compare the results of different stabilizers, the root mean square (RMS) error was calculated using the following equation:

$$RMS = \sqrt{\frac{\sum_{i=1}^{N}\left(d_i^{surface} - d_i^{downward}\right)^2}{N}} \quad (27)$$

where N is the number of data, and $d^{surface}$ and $d^{downward}$ represent the theoretical surface and downward continued data, respectively. Table 4 shows these RMS errors calculated from the use of different stabilizers. As it can be seen in the magnetic data, the RMS errors related to the βL_1, L_2, and MS stabilizers have the lowest values, respectively, while in the gravity data, the βL_1, MS, L_2, and SM stabilizers show better results.

Table 4. RMS errors related to different stabilizers in the synthetic data.

	RMS error							
Synthetic data	βL_1	L_1	L_2	SM	MS	MGS	ME-1	TV
Magnetic	15.74	19.54	16.71	17.86	17.12	18.57	37.65	24.10
Gravity	0.13	0.20	0.16	0.19	0.14	0.20	0.23	0.17

Another method used in this work to evaluate the results is a graphical comparison of data. In this procedure, the scatter plot of 150-m downward continued data versus surface theoretical data was drawn (Figures 4 and 7). In this method, the criterion of the superiority of one stabilizer over others is the conformity of the trend line of its scatter plot to the line x = y. As shown in Figure 4 (magnetic case), the degree of compliance with the x = y line is approximately equal in all plots but the extent of data dispersion varies. Thus another condition for choosing a stabilizer is to have a minimum width along the x = y line. Accordingly, Figures. 4a, 4d, and 4e that correspond to the βL_1, SM, and MS stabilizers, respectively, can be the candidates for the desired stabilizer. In the gravity example, the βL_1 and SM stabilizers have produced the best results (Figures. 7a, 7d).

4. Geological descriptions of Esfordi district

Different kinds of iron deposits including Kiruna-type magnetite-apatite, volcano-sedimentary, skarn, IOCG (i.e. iron oxide-copper-gold deposit), magmatic, and placer deposits are found in Iran [30]. In general, these deposits and indications are distributed in four major areas including Central Iran, Sanandaj–Sirjan zone, Eastern Iran, and Kordestan region [31]. One of the significant structural regions of Iran is the Bafgh-Posht-e-Badam block. This area is one of the components of the Central Iranian microcontinent based on newer structural divisions of Iran [32]. The Bafgh-Posht-e-Badam block, also known as the Bafgh metallogenic zone, is the place of occurrence of various iron deposits. Figure 8 shows the distribution map of the iron deposits over the tectonic map of Iran. As it can be seen, the concentration of these deposits in the Bafgh region is high.

The studied area is a part of the Bafgh metallogenic zone, which dates back to the Late Precambrian-Early Cambrian period in the geological time scale. In this respect, it is the oldest metallogenic zone of Iran [31]. The Esfordi district is located in the northeast of the city of Bafgh in the Yazd Province (Iran) between the 55˚30′ to 56˚00′ eastern longitudes and the 31˚30′ to 32˚00′ northern latitudes. A simplified geological map with iron and phosphate deposits of the Esfordi area is shown in Figure 9. In this district, different units outcrop from the Precambrian to Quaternary. The studies conducted by the Geological Survey of Iran (GSI) indicate that this area is economically prosperous. In this regard, the deposits and occurrences of iron, manganese, lead and zinc, apatite, molybdenum, copper, gypsum, and building stones have been reported. One of the prominent features of this region is the existence of numerous various iron deposits, which is an encouraging factor for applying the magnetometry method to explore the areas prone to iron mineralization and other associated minerals.

5. Application to real data set in Esfordi district

The Esfordi aeromagnetic data used for this work was collected under the supervision of the Geological Survey of Iran (GSI). The data was measured at an altitude of 150 m above the ground surface, and the distance between the flight lines was 560 m. The Aeromagnetic residual map over the Esfordi district is shown in Figure 10a. Also the reduced-to-pole (RTP), analytic signal (AS), and tilt angle maps are shown in Figures. 10b-d. The location of the known iron and phosphate deposits mentioned in Figure 9 have been superimposed on these maps.

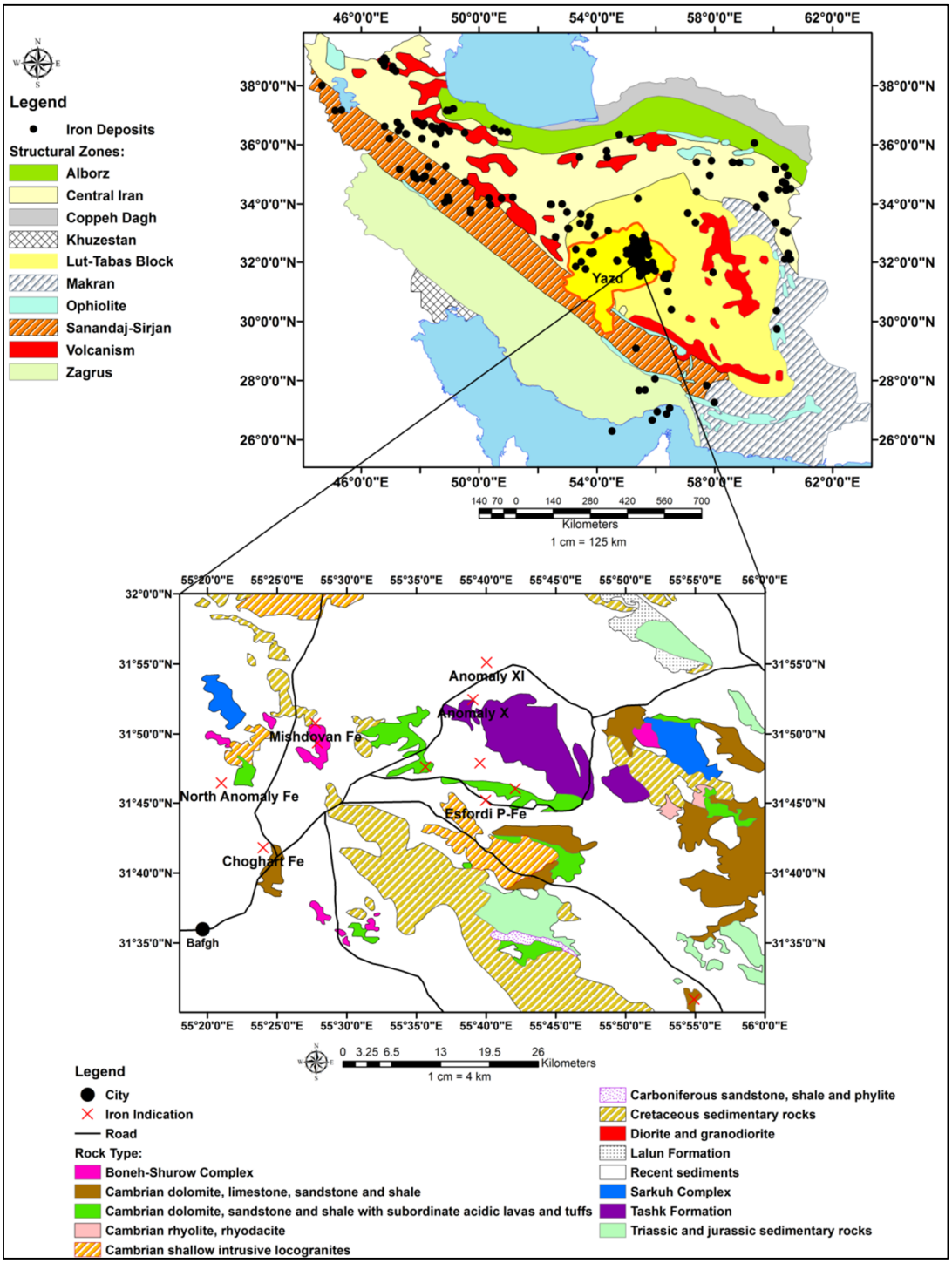

Figure 8. Distribution map of iron deposits over the tectonic map of Iran, where the location of the Esfordi district is shown in the middle of map (reproduced from [30, 31]).

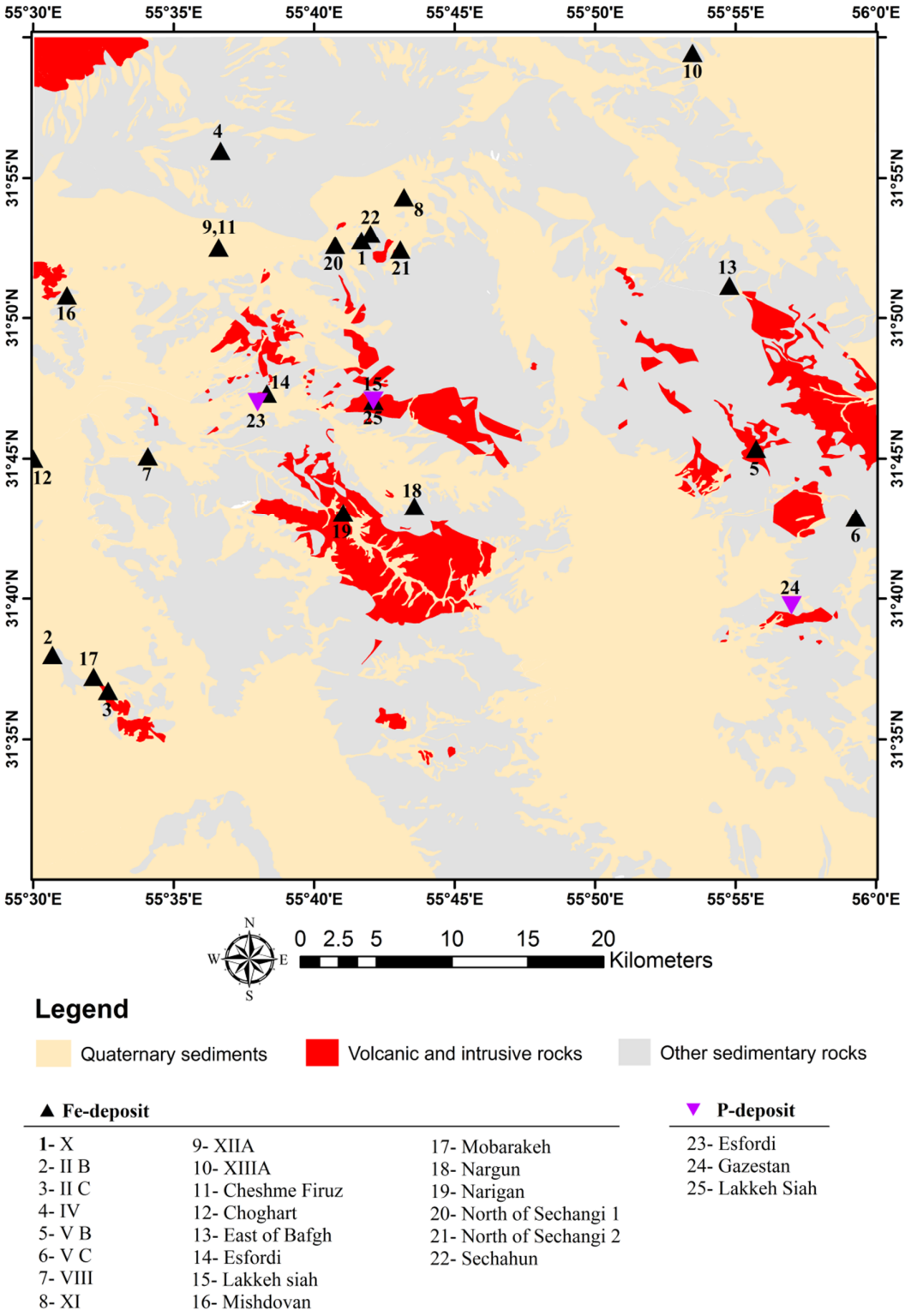

Figure 9. Simplified 1:100,000 scale geological and mineral occurrence map of the studied area located in the Esfordi district (reproduced from reports of the Geological Survey of Iran, GSI).

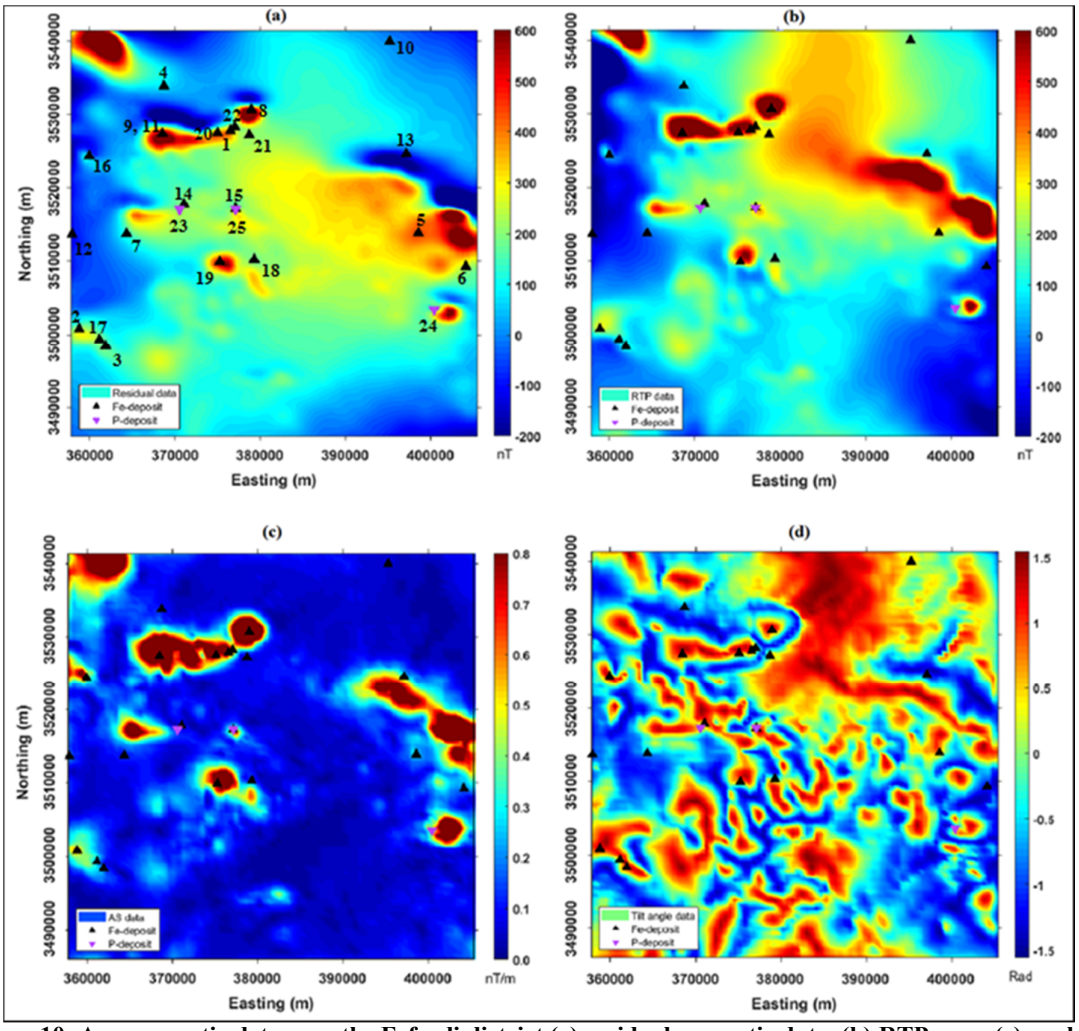

Figure 10. Aeromagnetic data over the Esfordi district (a) residual magnetic data, (b) RTP map, (c) analytic signal map, (d) tilt angle map. Locations of the Fe-P deposits listed in Table 2 have been superimposed on all maps.

As it can be seen, the analytical signal map has reliably identified the areas concerning the available deposits. By applying the Tikhonov regularization method and using different stabilizers, the 150-m downward continued maps were generated (Figure 11). For best results, the value of the optimum regularization parameter according to Figure 12 was selected from the L-curve method. As it can be seen, the results obtained are slightly different from the original data (Figure 10a) because the height difference between the two observation and continuation levels is not high. In this situation, the visual comparison was challenging to perform. Also due to the lack of sufficient information to validate the results, we decided to use a recursive approach in order to calculate the RMS error to evaluate the results. We performed the upward continuation operation similarly on the downward continued data. Then we used the original airborne data and the upward data to calculate the error. Therefore, the following equation was used:

$$RMS = \sqrt{\frac{\sum_{i=1}^{N}\left(d_i^{airborne} - d_i^{upward}\right)^2}{N}} \qquad (28)$$

In this equation, $d^{airborne}$ is the airborne data, d^{upward} is the upward data, and N is the number of data. The upward data was also calculated using Equation (3). Based on this, the RMS error values were calculated according to Table 5. As it can be seen in this case, the ME-1, L_1, MGS, and βL_1 stabilizers have a minor error compared to the others. Figures. 11c and 11d also confirm the high RMS error obtained from the L2 and SM stabilizers. For example, if we look at the position of No. 12 and 25 indices (Lakkeh siah Fe-P deposits), which are star-like, the downward

continued results show this area more strongly. At the same time, the L_2 norm and SM stabilizers have produced smoother results. Also the area related to the No. 18 index (i.e. Nargun Fe-deposit) confirms this issue. For this reason, these stabilizers can be excluded.

Table 5. RMS errors related to different stabilizers in the real data.

RMS error							
βL1	L1	L2	SM	MS	MGS	ME-1	TV
0.16	0.06	17.67	28.07	12.20	0.10	0.02	8.71

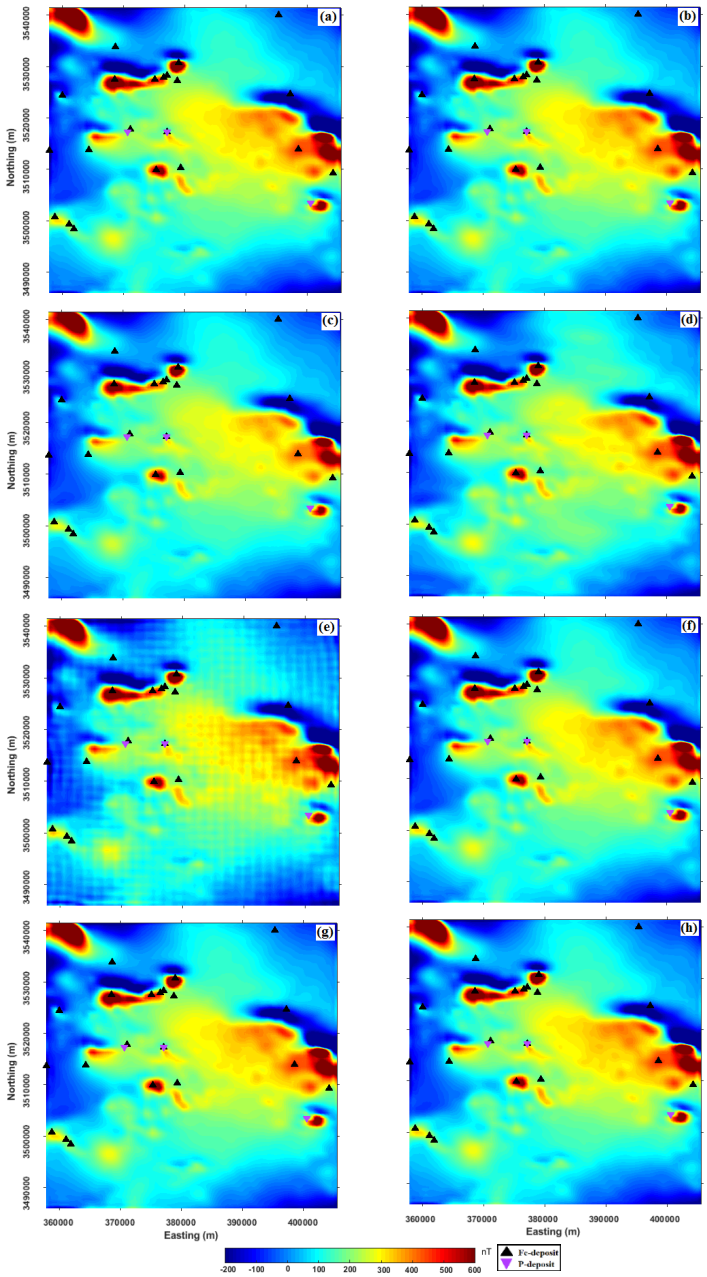

Figure 11. Downward continued magnetometry data over the Esfordi region through implementing a stabilizer of (a) βL_1, (b) L_1, (c) L_2, (d) SM, (e) MS, (f) MGS, (g) ME-1, and (h) TV. Locations of the Fe-P deposits have been superimposed on all maps.

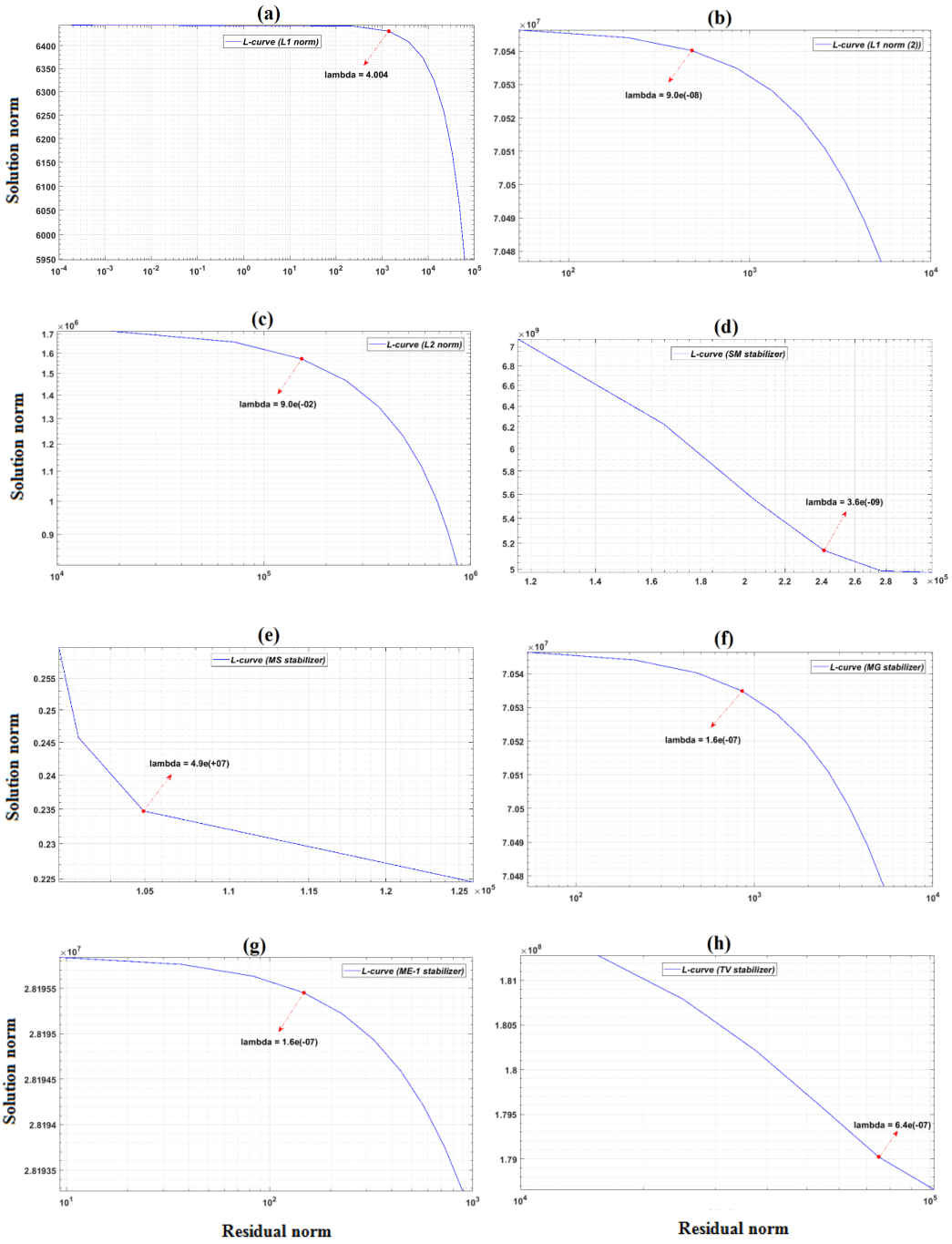

Figure 12. Selection of an optimum regularization parameter by means of the L-curve method for the various stabilizers of (a) βL_1, (b) L_1, (c) L_2, (d) SM, (e) MS, (f) MGS, (g) ME-1, and (h) TV. The magnetometry data over the Esfordi region was the input data for continuation to the ground surface.

The integrated geophysical methods can reduce the uncertainty arising from the single set geophysical data modeling, where the physical properties of magnetic susceptibility and density contrast can image most intricate geological targets through a fusion rule employed [33]. In the Esfordi region, since we have just access to the aeromagnetic data, the integrated approaches for target identification (i.e. iron deposit) were not possible to be utilized. We believe a multi-disciplinary geospatial data set comprising airborne geophysics, satellite imagery data along with geochemical, and geological data can lead to a more usable output [34, 35], and it deserves to be studied in a separate work.

6. Conclusions

In this work, we investigated the ability of various stabilizers to stabilize the downward continuation of the airborne data. This operation was performed by inserting the βL_1, L_1, L_2, SM, MS, MGS, ME-1, and TV stabilizers into the Tikhonov parametric function, and then by minimizing this function, the synthetic gravity and magnetic models were created in order to evaluate the efficiency of these stabilizers. The calculated downward continued data was then compared with the surface theoretical data. This comparison was made in three ways: visual method, quantitative method (calculation of RMS error), and graphical method. In the visual comparison, revealing all the anomalous sources while controlling the noise level was our criterion in selecting the best stabilizing functions. Based on this, the βL_1, L_2, SM, MGS, and TV stabilizers in the magnetic example and the βL_1, L_2, SM and TV stabilizers in the gravity example were among the candidates of most suitable stabilizers. In order to evaluate these results quantitatively, the amount of RMS error of different stabilizers was calculated. In this regard, based on having the slightest RMS error, the βL_1 (e = 15.74), L_2 (e = 16.71), and MS (e = 17.12) stabilizers in the magnetic case and the βL_1 (e = 0.13), MS (e = 0.14), L_2 (e = 0.16), and SM (e = 0.19) stabilizers in gravity case were introduced as the nominees for the best stabilizer. In the graphical method, the best results were determined based on the correspondence with the x=y line. The βL_1, SM, and MS stabilizers in the magnetic data and the βL_1 and SM stabilizers in the gravity data were introduced as the desired stabilizing functions by examining this condition. In addition, this work was performed on the real airborne magnetic data of the Esfordi district in the Yazd Province in Iran. In this case, the results obtained were evaluated by visually comparing the data and calculating the RMS error of different stabilizers in order to determine the most suitable stabilizer. Based on this, the ME-1, L_1, MGS, and βL_1 stabilizers with RMS error values of 0.02, 0.06, 0.1, and 0.16 could be introduced as the most suitable stabilizers. Considering all the results obtained from the synthetic and real examples, it can be concluded that the βL_1 stabilizer (the second definition of the L_1 norm) is a good choice to achieve the most appropriate results in the execution of a stable downward continuation operation.

Acknowledgements

The authors would like to express their sincere thanks to the School of Mining Engineering-University of Tehran for all supports, and the Geological Survey of Iran (GSI) for data and geological map provision.

References

[1]. Gandhi, S. and Sarkar, B. (2016). Essentials of mineral exploration and evaluation: Elsevier.

[2]. Revuelta, M.B. (2017). Mineral Resources: From Exploration to Sustainability Assessment: Springer.

[3]. Reynolds, J.M. (2011). An introduction to applied and environmental geophysics: John Wiley and Sons.

[4]. Hinze, W. J., Von Frese, R.R. and Saad, A.H. (2013). Gravity and magnetic exploration: Principles, practices, and applications: Cambridge University Press.

[5]. Zeng, X., Liu, D., Li, X., Chen, D. and Niu, C. (2014). An improved regularized downward continuation of potential field data. Journal of Applied Geophysics. 106: 114-118.

[6]. Abedi, M., Gholami, A. and Norouzi, G.H. (2013). A stable downward continuation of airborne magnetic data: A case study for mineral prospectivity mapping in Central Iran. Computers and Geosciences. 52: 269-280.

[7]. Liu, X., Li, Y., Xiao, Y., and Guan, B. (2015). Downward continuation of airborne geomagnetic data based on two iterative regularization methods in the frequency domain. Geodesy and Geodynamics. 6 (1): 34-40.

[8]. Mansi, A.H., Capponi, M. and Sampietro, D. (2018). Downward continuation of airborne gravity data by means of the change of boundary approach. Pure Applied Geophysics. 175, 977–988.

[9]. Pašteka, R., Karcol, R., Kušnirák, D., and Mojzeš, A. (2012). REGCONT: A Matlab-based program for stable downward continuation of geophysical potential fields using Tikhonov regularization. Computers and Geosciences. 49: 278-289.

[10]. Tikhonov, A.N. and Arsenin, V.Y. (1977). Solutions of Ill-Posed Problems, D.C. Winston, Washington.

[11]. Last, B. and Kubik, K. (1983). Compact gravity inversion. Geophysics. 48 (6): 713-721.

[12]. Constable, S.C., Parker, R.L. and Constable, C.G. (1987). Occam's inversion: A practical algorithm for generating smooth models from electromagnetic sounding data. Geophysics. 52 (3): 289-300.

[13]. Rudin, L.I., Osher, S. and Fatemi, E. (1992). Non-linear total variation-based noise removal algorithms. Physica D: non-linear phenomena. 60 (1-4): 259-268.

[14]. Ramos, F. M., Velho, H.F.C., Carvalho, J.C. and Ferreira, N.J. (1999). Novel approaches to entropic regularization. Inverse Problems. 15 (5): 1139.

[15]. Portniaguine, O. and Zhdanov, M.S. (1999). Focusing geophysical inversion images. Geophysics. 64 (3): 874-887.

[16]. Zhdanov, M.S. (2002). Geophysical inverse theory and regularization problems (Vol. 36): Elsevier.

[17]. Mehanee, S. and Zhdanov, M. (2002). Two-dimensional magnetotelluric inversion of blocky geoelectrical structures. Journal of Geophysical Research: Solid Earth. 107 (B4): EPM 2-1-EPM 2-11.

[18]. Candansayar, M.E. (2008). Two-dimensional inversion of magnetotelluric data with consecutive use of conjugate gradient and least-squares solution with singular value decomposition algorithms. Geophysical prospecting. 56 (1): 141-157.

[19]. Zhao, C., Yu, P. and Zhang, L. (2016). A new stabilizing functional to enhance the sharp boundary in potential field regularized inversion. Journal of Applied Geophysics. 135: 356-366.

[20]. Xiang, Y., Yu, P., Zhang, L., Feng, S. and Utada, H. (2017). Regularized magnetotelluric inversion based on a minimum support gradient stabilizing functional. Earth, planets and space. 69 (1): 158.

[21]. Gündoğdu, N.Y. and Candansayar, M.E. (2018). Three-dimensional regularized inversion of DC resistivity data with different stabilizing functionals. Geophysics. 83 (6): E399-E407.

[22]. Rezaie, M. (2019). 3D non-smooth inversion of gravity data by zero-order minimum entropy stabilizing functional. Physics of the Earth and Planetary Interiors. 294: 106275.

[23]. Dentith, M. and Mudge, S.T. (2014). Geophysics for the mineral exploration geoscientist: Cambridge University Press.

[24]. Blakely, R.J. (1995). Potential theory in gravity and magnetic applications: Cambridge university press.

[25]. Li, Y. and Devriese, S. (2009). Enhancement of magnetic data by stable downward continuation for UXO applications. In 79th Annual International Meeting, SEG (pp. 1464–1468).

[26]. Ma, G. Q., Liu, C., Huang, D.N. and Li, L.L. (2013). A stable iterative downward continuation of potential field data. Journal of Applied Geophysics. 98: 205–211.

[27]. Zhou, W., Li, J. and Yuan, Y. (2018). Downward Continuation of Potential Field Data based on Chebyshev-Pade´ Approximation Function. Pure Applied Geophysics. 175: 275–286.

[28]. Li, Y., Devriese, S.G., Krahenbuhl, R.A. and Davis, K. (2013). Enhancement of Magnetic Data by Stable Downward Continuation for UXO Application. IEEE Transactions on Geoscience and Remote Sensing. 51 (6): 3605-3614.

[29]. Hansen, P.C. and O'Leary, D.P. (1993). Use of the L-curve in the regularization of discrete ill-posed problems. SIAM journal on scientific computing, 14 (6): 1487-1503.

[30]. Nabatian, G., Rastad, E., Neubauer, F., Honarmand, M. and Ghaderi, M. (2015). Iron and Fe–Mn mineralization in Iran: implications for Tethyan metallogeny. Australian Journal of Earth Sciences. 62 (2): 211-241.

[31]. Ghorbani, M. (2013). Economic geology of Iran (Vol. 581): Springer.

[32]. Aghanabati, A. (2004). Geology of Iran. Geological survey of Iran.

[33]. Nasri, S., Nejati Kalate, A., Roshandel Kahoo, A., and Soleimani Monfared, M. (2020). New insights into the structural model of the Makran subduction zone by fusion of 3D inverted geophysical models. Journal of Asian Earth Sciences. 188: 104075.

[34]. Soleimani, M. and Jodeiri Shokri, B. (2016). Intrinsic geological model generation for chromite pods in the Sabzevar ophiolite complex, NE Iran. Ore Geology Reviews. 78: 138-150.

[35]. Riahi, Sh., Bahroudi, A., Abedi, M., Aslani, S. and Elyasi, Gh.R. (2021). Integration of airborne geophysics and satellite imagery data for exploration targeting in porphyry Cu systems: Chahargonbad district, Iran. Geophysical Prospecting, https://doi.org/10.1111/1365-2478.13092.

ادامه فروسوی پایدار داده ژئوفیزیکی میدان پتانسیل: بررسی خانواده پایدارکننده‌ها

مجید آزادی، میثم عابدی* و غلامحسین نوروزی

دانشکده مهندسی معدن، پردیس دانشکده‌های فنی، دانشگاه تهران، تهران، ایران

ارسال ۲۰۲۱/۰۴/۱۹، پذیرش ۲۰۲۱/۰۵/۲۱

* نویسنده مسئول مکاتبات: maysamabedi@ut.ac.ir

چکیده:

میرایی سیگنال دریافت شده از منابع ایجاد کننده بی‌هنجاری ویژگی منفی اندازه‌گیری‌های هوابرد است. استفاده از یک رهیافت ادامه فروسوی پایدار ابزاری عملی برای رفع این کاستی است. در این پژوهش، کارآیی توابع پایدارکننده متنوع جهت دستیابی به یک داده فروسوی پایدار بررسی خواهد شد. هدف از این کار، انتخاب مناسب‌ترین پایدارکننده(ها) برای این فرایند است. لذا توابع مختلف پایدارکننده با ادغام آن‌ها در معادله منظم‌سازی تیخونوف بررسی خواهیم شد. نتایج کار تحقیقاتی حاکی از این است که در مورد داده‌های مصنوعی گرانی‌سنجی و مغناطیس، پایدارکننده‌های $\beta L1$ (مشتق از نرم L1) و SM (نرمترین مدل) پتانسیل لازم جهت ادامه‌ی فروسوی پایدار را دارند. این پایدارکننده‌ها با مقایسه از سه طریق بصری، کمی (خطای RMS) و گرافیکی بهتر از سایرین عمل می کنند. همچنین با بررسی داده‌های هوابرد مغناطیسی منطقه اسفوردی در استان یزد (ایران)، مشخص شد که به طور کلی، پایدارکننده $\beta L1$ نسبت به سایر توابع پایدارکننده مطالعه شده در این کار تحقیقاتی، عملکرد بهتری دارد.

کلمات کلیدی: میرایی سیگنال، ادامه فروسوی پایدار، منظم‌سازی تیخونوف، توابع پایدارکننده.